engineering proceedings

MDPI

Proceeding Paper

Design of a Scissor-Structural Mechanism for a Morphing Missile Nose Cone †

Koray Özdemir [1,2,*] and Yavuz Yaman [1]

[1] Department of Aerospace Engineering, Middle East Technical University, 06800 Ankara, Turkey; yyaman@metu.edu.tr
[2] Roketsan A.Ş., 06780 Ankara, Turkey
* Correspondence: ozdemir.koray@metu.edu.tr
† Presented at the 15th EASN International Conference, Madrid, Spain, 14–17 October 2025.

Abstract

In this paper, the design of a novel deployable scissor-structural mechanism (SSM) for the morphing of a generic missile nose cone is presented. The aim of the study is to explore a geometric transformation specially designed for the missile's flight envelope, ensuring optimal aerodynamic performance and decreasing the aerodynamic drag coefficient across different flight conditions, then to apply it. For the geometric transformation the proposed mechanism is composed of multiple scissor-like elements (SLEs), providing a reconfigurable structure capable of adjusting the nose cone shape dynamically. To achieve a continuous and smooth missile nose cone surface the study incorporates a superelastic alloy (SEA) skin, which can deform compatibly with the SLE movements. A computational routine provides the study with an optimum SSM configuration which makes the geometric transformation the best. The computational routine minimizes the structural error between deformed nose cone shape and target nose cone shape.

Keywords: morphing missile nose cone; aerodynamic drag coefficient; aerodynamic performance

1. Introduction

Morphing aircraft are capable of substantially changing their external shape to adapt to diverse mission environments which gives them a multi-role characteristic [1]. Morphing technology in aircraft has become popular in modern aviation. The main motivation behind morphing technology is to change the geometry of an aircraft in an effort to adapt to varying mission requirements and flight conditions. Unlike conventional fixed-geometry designs, aircraft with morphing technology are superior as they have improved aerodynamic efficiency and mission adaptability due to their controlled morphing which increases the characteristic of multi-role identity.

Morphing technology offers great improvements in missile performance also, which incentivizes its application in some novel missile designs. One application is MUTANT, Missile Utility Transformation via Articulated Nose Technology, by The U.S. Air Force Research Laboratory (AFRL). The aim is to significantly improve missile range and lethality against highly maneuverable targets with a better flight control actuation system. Its method of shape transformation, which can be seen in Figure 1, is composed of active morphing, involving high-rate pivoting of the missile forebody, referred to as articulation [2]. In literature different morphing methods are also available. One study offers a morphing

Check for updates

Academic Editors: Spiros Pantelakis, Andreas Strohmayer and Gustavo Alonso

Published: 7 May 2026

Copyright: © 2026 by the authors. Licensee MDPI, Basel, Switzerland. This article is an open access article distributed under the terms and conditions of the Creative Commons Attribution (CC BY) license.

nose cone using a slider-crank mechanism to change the bluntness of the nose cone for atmospheric reentry vehicles [3]. Another study offers a biomimetic skeleton structure capable of telescoping and bending to morph the nose cone of aerospace vehicles [4].

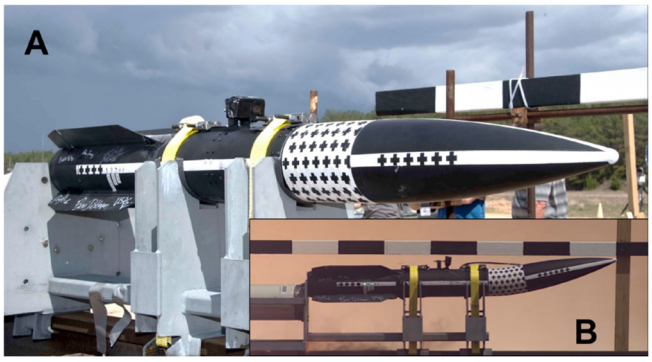


Figure 1. (**A**) First generation articulation system integrated into Hellfire body; (**B**) High-speed snapshot during test where forebody actively articulates [2].

Length-to-Diameter ratio (length of missile nose cone/diameter of missile) —fineness ratio—is an aerodynamic phenomenon which defines the ratio of missile nose cone length to nose cone diameter. In missiles with a higher fineness ratio, pressure gradient is less severe which results in a lower pressure drag in the nose. Figure 2 shows the relation between fineness ratio and axial drag force coefficient (CA) for fixed diameter, length, and nose cone profile missiles with different nose cone lengths. It is seen that higher fineness ratio offers improved aerodynamic performance, decreasing axial force coefficient (CA) [5].

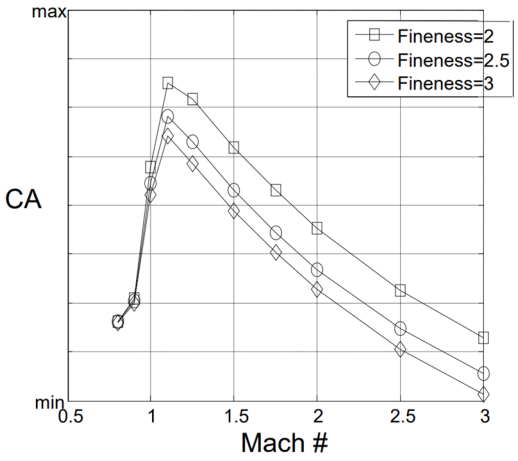


Figure 2. Change in axial force coefficient with nose fineness across different Mach numbers, # [5].

It is better to design the missile with a higher fineness ratio, but engineering requirements do not allow it. Missile dimensions are strictly constrained by several factors. For ground-based missiles, the dimensions can be constrained by canister or carrying vehicle sizes. The system must be kept as compact as possible. As the system gets smaller, it has better transportability. When it gets bigger, it is harder to find suitable transportation means. Even if there can be means, they will undoubtedly be more expensive. For air-launched missiles, compact ones are clearly better options for aircraft weapon stations. By means of narrow internal weapon stations, compact ones fit better. By means of external stations, compact missiles are safer for take-off and landing. On the other hand, they have a lower radar cross-section (RCS).

The novel approach is to morph missile nose cone using SSM, fitted inside the nose cone, which can make the nose cone elongate and shorten through the missile axis. It

enables a missile to have a nose cone with low fineness ratio, which ensures easier storage and transportation, and the ability to elongate the missile nose cone after the launch to have smaller CA; this elongation makes the missile fly with lower aerodynamic drag.

There is another advantage of the mechanism. The mechanism offers two different nose cones with different CAs. When missiles try to fit on their planned trajectories, they can make high-g maneuvers to brake. When brakes are needed, this mechanism can get back to its higher CA design using reverse actuation enabling better brake performance. This reverse actuation can decrease the acceleration of the brake maneuver which decreases aerodynamic structural load.

2. Methodology

The novel morphing mechanism is composed of multiple SLEs. For this study, the mechanism is designed to work in 2-D. A set of SLEs linked together side by side forms the SSM. A generic SLE is given in Figure 3. All SLEs are linked side by side together from the nodes on t-lines forming the SSM. Then the skin is assumed to be linked to the nodes on t-lines and it is deformed via the movement of those nodes. All links can be split into two segments with different lengths by pivots.

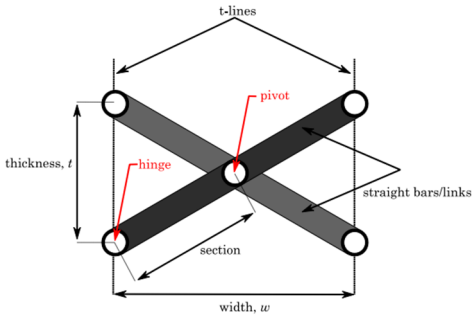


Figure 3. A basic scissor-like element [6].

The mechanism works as a 1 DOF system. For elongation, it is actuated by decreasing the distance between the symmetric actuated nodes by following the downward red arrow in Figure 4. For shortening, it is actuated by increasing the distance between the symmetric actuated nodes to get back to its initial position by following the upward red arrow in Figure 4. These actuations elongate or shorten the nose skin, assumed to be able to deform continuously, by pushing or pulling it from the nodes on t-lines.

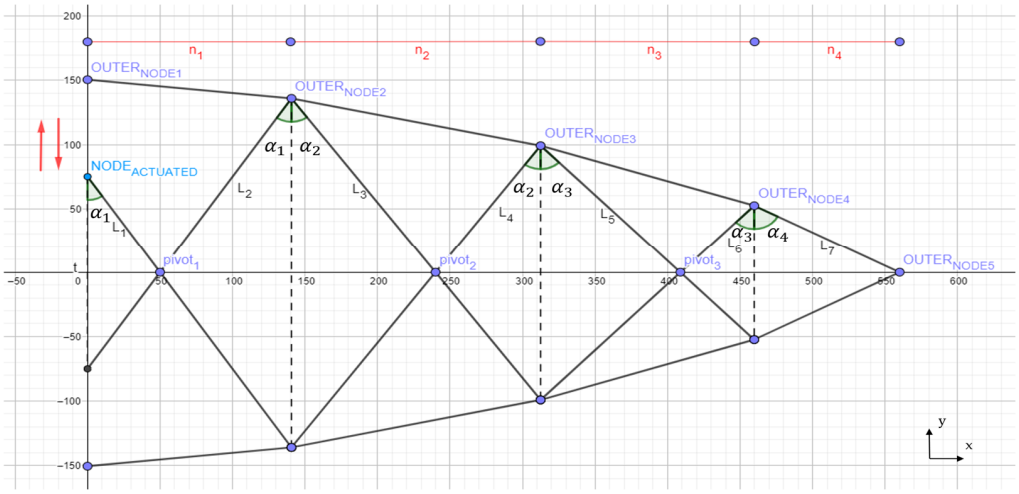


Figure 4. A sample of SSM with 4 SLEs.

In Figure 4 a sample of SSM integrated into a nose cone is illustrated. In Figure 4, there are 4 SLEs. In the study the last SLEs are assumed to have a left-half segment before the pivot. Once link lengths are determined (in this sample $L_1 \ldots L_7$ for 4 SLEs in which the mirror lengths are the same), outer nodes are moved in a 1 DOF system in which the actuated node and its mirror about the missile axis move vertically causing the skin to deform compatibly with the outer nodes. Link lengths are dependent on actuated node position (before actuation), nose cone profile (assumed to be always positive), and how the nose cone length is segmented (in this sample it is segmented as $n_1 \ldots n_4$).

$$x_{n_1} = n_1, \tag{1}$$

$$x_{n_2} = n_1 + n_2, \tag{2}$$

$$x_{n_3} = n_1 + n_2 + n_3, \tag{3}$$

$$x_{n_4} = n_1 + n_2 + n_3 + n_4, \tag{4}$$

$$y_{n_1} = y_{nose\ cone\ profile}(x_{n_1}), \tag{5}$$

$$y_{n_2} = y_{nose\ cone\ profile}(x_{n_2}), \tag{6}$$

$$y_{n_3} = y_{nose\ cone\ profile}(x_{n_3}), \tag{7}$$

$$y_{n_4} = y_{nose\ cone\ profile}(x_{n_4}), \tag{8}$$

$$\alpha_1 = tan^{-1}\left[\frac{y_{n_1} + y_{actuated_{node}}}{x_{n_1}}\right], \tag{9}$$

$$L_1 = \frac{y_{actuated_{node}}}{cos\alpha_1}, \tag{10}$$

$$L_2 = \frac{y_{n_1}}{cos\alpha_1}, \tag{11}$$

$$\alpha_2 = tan^{-1}\left[\frac{y_{n_2} + y_{n_1}}{x_{n_2} - x_{n_1}}\right], \tag{12}$$

$$L_3 = \frac{y_{n_1}}{cos\alpha_2}, \tag{13}$$

$$L_4 = \frac{y_{n_2}}{cos\alpha_2}, \tag{14}$$

$$\alpha_3 = tan^{-1}\left[\frac{y_{n_3} + y_{n_2}}{x_{n_3} - x_{n_2}}\right], \tag{15}$$

$$L_5 = \frac{y_{n_2}}{cos\alpha_3}, \tag{16}$$

$$L_6 = \frac{y_{n_3}}{cos\alpha_3}, \tag{17}$$

$$\alpha_4 = tan^{-1}\left[\frac{y_{n_4} + y_{n_3}}{x_{n_4} - x_{n_3}}\right], \tag{18}$$

$$L_7 = \frac{y_{n_3}}{cos\alpha_4}, \tag{19}$$

The SSM is integrated into a nose cone with the formulas above. The deformed skin shape is determined by actuated outer nodes. The positions of actuated outer nodes depend

https://doi.org/10.3390/engproc2026133082

solely on the position of the actuated node (after actuation). For the sample in Figure 4, the outer node positions are determined using the formulas below:

$$x_{outer\ node\ 1} = 0, \tag{20}$$

$$y_{outer\ node\ 1} = radius\ of\ the\ nose\ cone, \tag{21}$$

$$\alpha_1^* = cos^{-1}\left[\frac{y^*_{actuated_{node}}}{L_1}\right], \tag{22}$$

$$x_{outer\ node\ 2} = x_{outer\ node\ 1} + (L_1 + L_2)sin\alpha_1^*, \tag{23}$$

$$y_{outer\ node\ 2} = L_2 cos\alpha_1^*, \tag{24}$$

$$\alpha_2^* = cos^{-1}\left[\frac{L_2 cos\alpha_1^*}{L_3}\right], \tag{25}$$

$$x_{outer\ node\ 3} = x_{outer\ node\ 2} + (L_3 + L_4)sin\alpha_2^*, \tag{26}$$

$$y_{outer\ node\ 3} = L_4 cos\alpha_2^*, \tag{27}$$

$$\alpha_3^* = cos^{-1}\left[\frac{L_4 cos\alpha_2^*}{L_5}\right], \tag{28}$$

$$x_{outer\ node\ 4} = x_{outer\ node\ 3} + (L_5 + L_6)sin\alpha_3^*, \tag{29}$$

$$y_{outer\ node\ 4} = L_6 cos\alpha_3^*, \tag{30}$$

$$\alpha_4^* = cos^{-1}\left[\frac{L_6 cos\alpha_3^*}{L_7}\right], \tag{31}$$

$$x_{outer\ node\ 5} = x_{outer\ node\ 4} + L_7 sin\alpha_4^*, \tag{32}$$

$$y_{outer\ node\ 5} = 0 \tag{33}$$

where * represents the state after actuation. Formulas (1)–(33) make a clear analogy for different parameters.

3. Optimization Algorithm

In the previous section, a sample SSM is fitted into a sample nose cone to show the relations between dependent and independent parameters. In the main optimization algorithm, it is aimed at finding an optimum SSM integrated into a generic missile nose cone which will fit to target geometry the best when actuated.

3.1. Selection of Base and Target Geometries

As base geometry, dimensions of one of the missiles produced by Roketsan are used. The nose cone geometry is a tangent-ogive profile with 300 mm diameter and 3 fineness ratio. In the algorithm it is aimed to elongate the nose cone and to have, again, a tangent-ogive geometry, but this time with 4 fineness ratio. During morphing, the skin is assumed to be moved because of the outer nodes illustrated in Figure 4 which connect the mechanism to the skin. Base and target geometries are plotted in Figure 5.

https://doi.org/10.3390/engproc2026133082

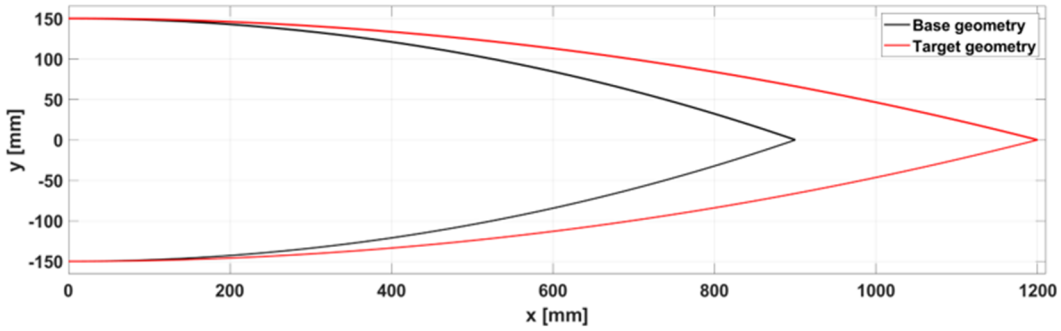


Figure 5. Base and target geometries.

3.2. Iteration Parameters

The algorithm needs three independent parameters. To integrate the SSM into base geometry, it needs n, number of SLEs (it is assumed that the SLEs split the nose cone length into n equal segments), and actuated node position (before actuation). n is iterated between 2 and 15 while actuated node position (before actuation) is iterated between 50 mm and 130 mm. Using Equations (1)–(19) link lengths for every iteration couples of n and actuated node positions (before actuation) are determined by fitting the SSM into base geometry. In Figure 6, the integrated SSM exists. Then the third parameter is needed for actuation. The third parameter, which is actuated node position (after actuation), is iterated between 10 mm and actuated node position (before actuation)-1 mm.

3.3. Kinematic Deployment

Using actuated node position (after actuation) and link lengths, which are determined by the other parameters, for every parameter triples of n actuated node position before actuation and actuated node position after actuation, positions of outer nodes are determined using Equations (20)–(33).

3.4. Deployed Skin

The sequence of outer nodes in the deployed state is assumed to be connected linearly with piecewise-straight segments. This yields the new external nose sketch which is the scissor-induced shape that elongates the base geometry without changing the base diameter. Figure 7 shows target geometry and corresponding outer skin.

3.5. Comparison of Deployed and Target Geometries

To determine what configuration is the best fit to target geometry, an error calculator part is added to the algorithm. This part splits both target sketch and the deployed sketch into n equal segments in length. Then, x coordinates and y coordinates (where the x coordinate intersects the sketch) are collected for both target sketch and deployed sketch. After that, using those coordinates, root-mean-square error, RMSE, is calculated for all combinations. Figure 8 shows those coordinates.

$$\boldsymbol{RMSE} = \left[\frac{\sum_{i=1}^{n} \left[\left| y_{target} - y_{deployed} \right|^2 + \left| x_{target} - x_{deployed} \right|^2 \right]}{\boldsymbol{n}} \right]^{0.5} \quad (34)$$

3.6. Optimization Result

The algorithm finds the combination with the least RMSE for the best fit and gives the parameters. The parameter set which gives the best fit is n = 15, actuated node position

(before actuation) = 62 mm and actuated node position (after actuation) = 60 mm. The corresponding RMSE is 6.0276 mm.

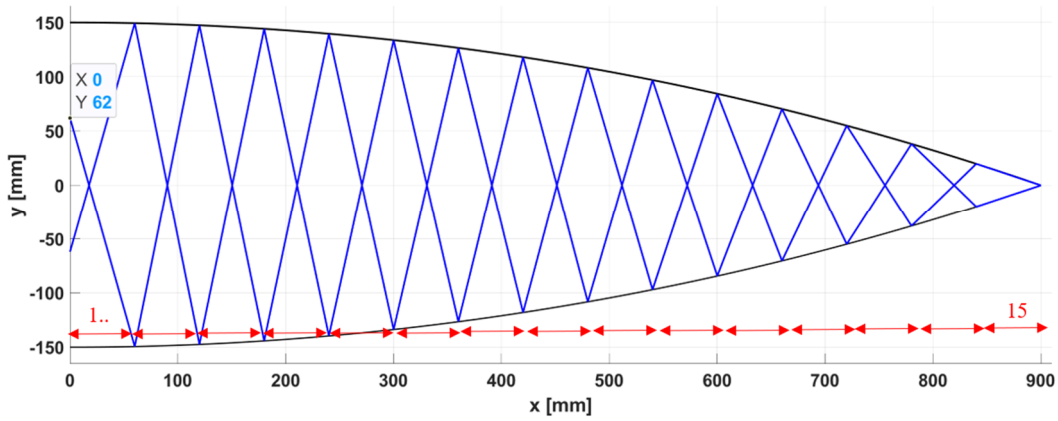


Figure 6. The SSM given by the algorithm before morphing with 15 SLEs, initial actuated node position y = 62 mm, final actuated node position y = 60 mm, and base geometry.

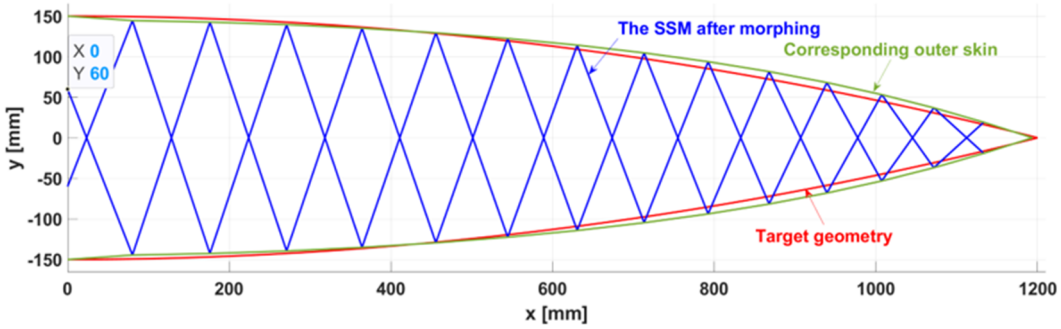


Figure 7. The SSM after morphing, corresponding outer skin and target geometry.

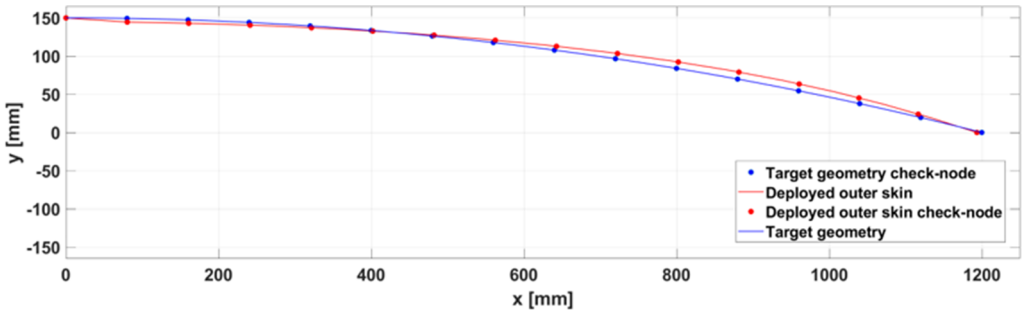


Figure 8. Deployed outer skin check-nodes and target geometry check-nodes for RMSE.

4. Effect of Morphing on Missile Performance

In order to compare range and hitting performances of base geometry (L/D = 3) and deployed geometry (L/D ≈ 4), for the two geometries CA values in different Mach numbers (up to 10 Mach) are taken from Missile DATCOM (although the mechanism is designed in 2-D, the geometries are assumed as 3-D, axially symmetric in Missile DATCOM). Time to morph is neglected, that is the base and the deployed geometries are evaluated as if they are different missiles because the morphing occurs just after the launch. Then, the performances of the geometries are compared via a 3-DOF algorithm. This algorithm treats the geometries as if they are a point. The points are launched at 45° with a thrust profile provided by Roketsan. They fly in a ballistic trajectory. An atmosphere model provided

by Roketsan is also included. The algorithm prints the trajectories and the hitting Mach numbers to see which one has the better performance. The forces acting on the points are illustrated in Figure 9.

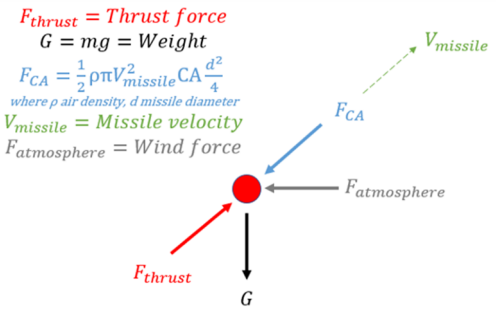


Figure 9. Forces acting on the missile modeled as a point while ascending.

5. Results

Figure 10 shows that at the end of flight, the conceptual morphing design has a higher velocity which means it will hit the objective faster. Figure 11 shows that the conceptual morphing design results in better range performance. The morphing geometry offers about 10% improvement in both range and hitting performances. Therefore, while the missile can hit objectives at longer distances it can show better performance against anti-missiles by hitting the objective faster.

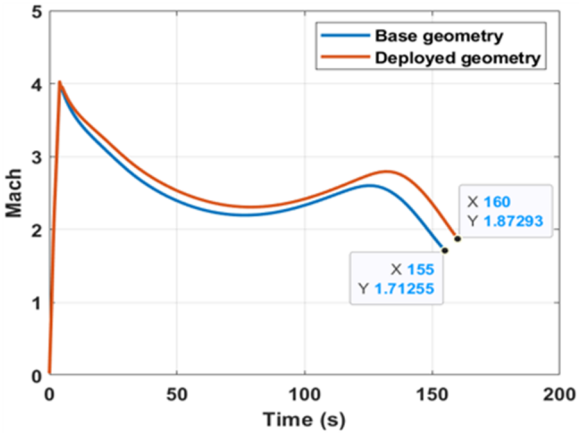


Figure 10. Mach vs. Time Plots.

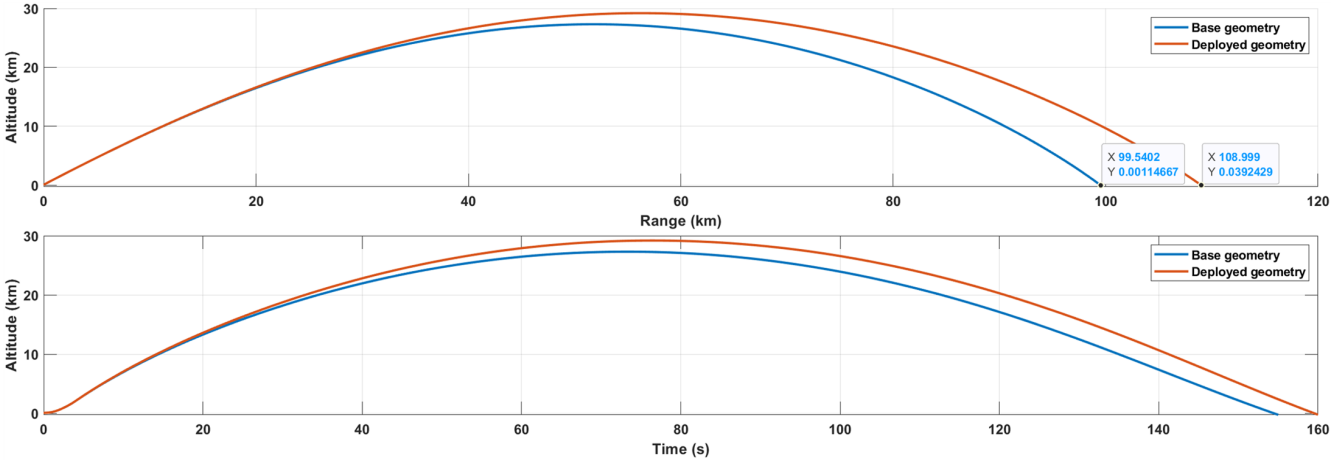


Figure 11. Altitude vs. Range and Altitude vs. Time Plots.

https://doi.org/10.3390/engproc2026133082

The primary concern of this research is on the kinematic and structural design of an SSM fitted inside a generic missile nose cone. Although the paper focuses on a missile nose cone as a case study, the underlying innovation is to offer morphing control surfaces applicable to a wide range of flight vehicles. The proposed method is flexible with the geometry in which the kinematic system is fitted. While the geometry can be a missile nose cone shape, it can also be an aircraft control surface, such as an aileron, rudder, or elevator.

Author Contributions: The study is carried out by K.Ö. The study is supervised by Y.Y. All authors have read and agreed to the published version of the manuscript.

Funding: This research received no external funding.

Institutional Review Board Statement: Not applicable.

Informed Consent Statement: Informed consent was obtained from all subjects involved in the study.

Data Availability Statement: Data is kept confidential by Roketsan.

Conflicts of Interest: The authors declare no conflicts of interest.

Dual-Use Statement: Current research is limited to the aerospace field which is beneficial for enhancing aerodynamic efficiency in flight vehicles and does not pose a threat to public health or national security. Authors acknowledge the dual use potential of the research involving morphing structures and confirm that all necessary precautions have been taken to prevent potential misuse. As an ethical responsibility, authors strictly adhere to relevant national and international laws about Dual-Use Research of Concern. Authors advocate for responsible deployment, ethical considerations, regulatory compliance, and transparent reporting to mitigate misuse risks and foster beneficial outcomes.

References

1. Weisshaar, T.A. Morphing Aircraft Technology—New Shapes for Aircraft Design. In *Multifunctional Structures/Integration of Sensors and Antennas, Meeting Proceedings RTO-MP-AVT-141, Overview 1*; RTO: Neuilly-sur-Seine, France, 2006; pp. O1-1–O1-20.
2. AFRL. MUTANT, Missile Utility Transformation via Articulated Nose Technology. 2023. Available online: www.afresearchlab.com (accessed on 5 September 2025).
3. Li, J.; Wu, J.; Yan, S. Conceptual design of deployment structure of morphing nose cone. *Adv. Mech. Eng.* **2013**, *2013*, 590957. [CrossRef]
4. Zhang, Y.; Zhao, J.; Chen, W.; Guo, X.; Yan, S.; Hu, G.; Yuan, Y.; Guo, P.; Cai, Q. Biomimetic skeleton structure of morphing nose cone for aerospace vehicle inspired by variable geometry mechanism of honeybee abdomen. *Aerosp. Sci. Technol.* **2019**, *92*, 405–416. [CrossRef]
5. Başoğlu, O.; Baran, Ö.U. Design and optimisation of high speed projectile nose for maximum effectiveness and stability. In Proceedings of the 7th Ankara International Aerospace Conference, METU, Ankara, Turkey, 11–13 September 2013.
6. Şahin, H.L.; Yaman, Y. Design and Analysis of a Novel Mechanism for the Morphing of Trailing Edge of an Aircraft Wing. In Proceedings of the 5th International Conference of Engineering Against Failure (ICEAF-V 2018), MATEC Web of Conferences, EDP Sciences, Chios, Greece, 20–22 June 2018. [CrossRef]

Disclaimer/Publisher's Note: The statements, opinions and data contained in all publications are solely those of the individual author(s) and contributor(s) and not of MDPI and/or the editor(s). MDPI and/or the editor(s) disclaim responsibility for any injury to people or property resulting from any ideas, methods, instructions or products referred to in the content.